

## Molecular Probes

## Complex-Formation-Enhanced Fluorescence Quenching Effect for Efficient Detection of Picric Acid

Aixiang Ding,<sup>[a]</sup> Longmei Yang,<sup>[a]</sup> Yuyang Zhang,<sup>[a]</sup> Gaobin Zhang,<sup>[a]</sup> Lin Kong,<sup>[a]</sup> Xuanjun Zhang,<sup>\*,[b]</sup> Yupeng Tian,<sup>[a, c]</sup> Xutang Tao,<sup>[c]</sup> and Jiaxiang Yang<sup>\*,[a, c]</sup>

**Abstract:** Amine-functionalized  $\alpha$ -cyanostilbene derivatives (Z)-2-(4-aminophenyl)-3-(4-butoxyphenyl)acrylonitrile (ABA) and (Z)-3-(4-butoxyphenyl)-2-[4-(butylamino)phenyl]acrylonitrile (BBA) were designed for specific recognition of picric acid (PA), an environmental and biological pollutant. The 1:1

host-guest complexes formed between the chemosensors and PA enhanced fluorescence quenching, thus leading to sensitive and selective detection in aqueous media and the solid phase.

## Introduction

The development of highly selective and sensitive sensors for the detection of high explosives, such as 2,4,6-trinitrotoluene (TNT), 2,4-dinitrotoluene (DNT), and picric acid (PA), has attracted much attention in the areas of national security and environmental protection.<sup>[1]</sup> Among various explosives, PA has far-ranging use in military facilities; in the leather, pharmaceutical, and blasting industries; and as sensitizers.<sup>[2]</sup> Moreover, PA causes chronic toxification owing to its potential damage to organs such as the respiratory system and the liver.<sup>[3]</sup> Therefore, PA has been recognized as an environmental and biological pollutant owing to the large amounts that are released into the environment upon degradation and its explosive, toxic nature. Many molecular and modulated chemosensors have been developed to meet the demand for the specific detection of PA.<sup>[4]</sup> Among them, fluorescent chemosensors would be a better choice on the basis of selectivity, sensitivity, simplicity, real-time feasibility, and the ability to be employed in both solution and the solid state. To date, various fluorescent materials have been developed as chemosensors for the detection of PA,

including film sensors,<sup>[5]</sup> pentacenequinone derivatives,<sup>[6]</sup> polymers,<sup>[7]</sup> nanofibers,<sup>[8]</sup> nanoparticles,<sup>[9]</sup> and so forth. Among them, aromatic amino compounds showed a clear capacity to combine with PA, thereby resulting in selective fluorescence quenching.<sup>[10]</sup> In particular, those connected to  $\pi$ -conjugated moieties would be fascinating tools in the field of optical sensing. Although some aromatic amine derivatives showed good selectivity and sensitivity, the structures of those sensor molecules are relatively complicated, and they usually require a complex, multistep synthetic procedure. Furthermore, most of the reported fluorescent chemosensors for PA function in pure organic media, which limits their practical application in the environmental detections. Hence, the remaining challenge for the detection of PA in water is to develop fluorescent chemosensor materials with simplicity and high efficiency.

In recent years  $\alpha$ -cyanostilbene derivatives have been involved in deeply studied and widely used fluorescent dyes,<sup>[11]</sup> but there are very few reports focused on the sensing field of neutral molecules. Intrigued by its remarkable fluorescent properties, in this work we have combined  $\alpha$ -cyanostilbene with amine or secondary amine to design small molecular probes (Z)-2-(4-aminophenyl)-3-(4-butoxyphenyl)acrylonitrile (ABA) and (Z)-3-(4-butoxyphenyl)-2-[4-(butylamino)phenyl]acrylonitrile (BBA), which are expected to form ionic pairs with PA and give effective fluorescence quenching (Scheme 1). The synthetic routes are shown in Scheme 2, and the single-crystal-line data of the corresponding compounds are summarized in Tables S1 and S2 of the Supporting Information. Herein, we report their sensing behaviors. In particular, their sensitivity and selectivity were compared.

## Results and Discussion

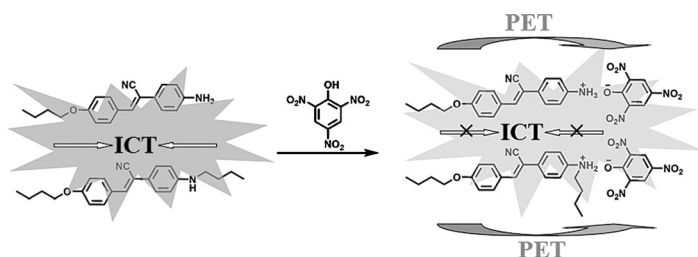
We first studied the optical properties of ABA and BBA in varying solvents. Both probes exhibit two characteristic absorption bands (Figure S2 in the Supporting Information). In the shorter-wavelength (about 300 nm) region, both of the probes

[a] Dr. A. Ding, L. Yang, Y. Zhang, Dr. G. Zhang, Prof. L. Kong, Prof. Y. Tian, Prof. J. Yang  
Department of Chemistry, Key Laboratory of Functional Inorganic Materials of Anhui Province  
Anhui University, Hefei 230039 (P.R. China)  
Fax: (+86)551-63861279  
E-mail: jxyang@ahu.edu.cn

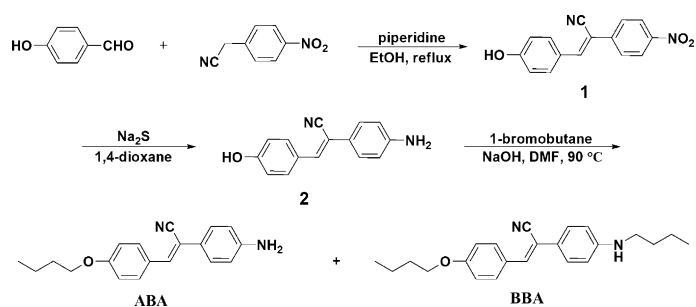
[b] Dr. X. Zhang  
Division of Molecular Surface Physics and Nanoscience  
Department of Physics, Chemistry, and Biology  
Linköping University, Linköping 58183 (Sweden)  
Fax: (+46)13-288969  
E-mail: xuazh@ifm.liu.se

[c] Prof. Y. Tian, Prof. X. Tao, Prof. J. Yang  
State Key Laboratory Materials  
Shandong University, Jinan 502100 (P.R. China)

Supporting information for this article is available on the WWW under <http://dx.doi.org/10.1002/chem.201402790>.



**Scheme 1.** Schematic illustration of the intermolecular interaction mode (ICT = intramolecular charge transfer) and the fluorescence quenching (PET = photoinduced electron transfer).



**Scheme 2.** Synthetic route to probes ABA and BBA.

show similar absorption, which changes little with polar variation of the solvents. This band can be ascribed to the  $\pi-\pi^*$  transitions. Whereas the intramolecular charge-transfer (ICT)-generated longer-wavelength absorption region clearly changed and was generally redshifted as the solvent polarity increased. The fluorescence results of the probes also exhibited a gradually redshifted phenomenon as the solvent polarity increased. The solid fluorescence of ABA and BBA is shown in Figure S3 of the Supporting Information. The analyzed results of the molecular structures indicated that the dihedral angles of the benzene rings of ABA and BBA were 51.06 and 22.32°, respectively. Thus, BBA was endowed with a better coplanar spatial structure and more widely delocalized electronic structure. Because of that, BBA (503 nm) showed a longer emission wavelength than ABA (480 nm).

To determine and expand the practical applications of these probes, we checked the emission properties in THF/water mixed solutions. As shown in Figure 1, the photoluminescence (PL) intensities of ABA and BBA show strong signals that were recorded at 465 and 473 nm, respectively. With an increase in the water fraction ( $f_w$ ), ABA showed a dramatic change in fluorescence intensity, which reached maximum at a  $f_w$  value of 10%. However, a further increase in  $f_w$  in the binary system led to a slow decrease in the emission intensity. The emission intensity nearly reached the initial state when  $f_w$  reached 70%, with the emission peak redshifted by 39 nm from 465 to 504 nm. In sharp contrast, the emission intensity of BBA changed little in the  $f_w$  range of 0–60% with the exhibition of a bathochromic effect, shifting by 38 nm from 473 to 511 nm. In this case, we decided to take advantage of the  $f_w$  of 70%

(ABA) and  $f_w$  of 60% (BBA) binary system for the detection of PA.

The fluorescence studies of ABA and BBA with PA, TNT, DNT, 1,3-dinitrobenzene (DNB), *p*-nitrotoluene (*p*-NT), 1,4-benzoquinone (BQ), nitromethane (NM), 2,3-dimethyl-2,3-dinitrobutane (DMDNB), nitrobenzene (NB), *p*-nitrochlorobenzene (*p*-NLB), and 1,4-cyclohexanedione (CHD) were carried out in the THF/H<sub>2</sub>O system. Among various nitro derivatives tested, probe ABA and BBA both showed selectivity and sensitivity toward PA. We examined the variation in UV/Vis absorption spectra of ABA and BBA in a mixture of water/THF (70% for ABA, 60% for BBA) with increasing amounts of PA. There were gradual enhancements in the two characteristic absorption bands, which indicated the interaction between ABA/BBA and PA (Figure S4 in the Supporting Information). The absorption spectra of the two probes in each binary system also exhibit two main peaks (located in band 1 and band 2, respectively). Upon addition of PA, the absorption at band 1 and band 2 both gradually in-

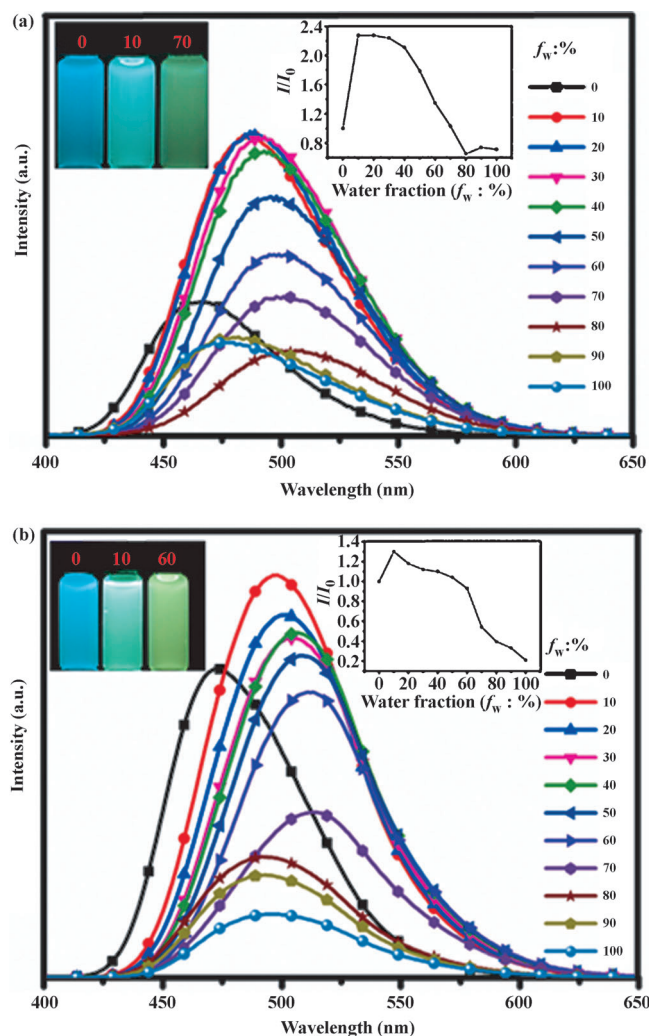


**Figure 1.** FL spectra of a) ABA and b) BBA in H<sub>2</sub>O/THF mixtures. Inset, upper left: Photographs recorded under 365 nm light in different water fractions. Inset, upper right: Plots of PL peak intensity versus water fraction ( $f_w$ ).

creased, and band 1 redshifted. By contrast, a linear relationship between the ratio of the absorbance ( $A_{\text{band}2}/A_{\text{band}1}$ ) and the concentration of PA in the range 0–20  $\mu\text{M}$  was observed, thus indicating that the probes could be applied for accurate colorimetric detection of detailed traces of PA in the environment.

Nearly 97% quenching of fluorescence emission occurred when one equivalent of PA was added to the binary solution of ABA, thus showing excellent sensing of PA. Nevertheless, only 38.7% fluorescence quenching was observed for BBA upon addition of one equivalent of PA (Figure 2). The fluorescence quenching process could also be observed by the naked eye (Figure 2, insets). As shown in Figure 3, Stern–Volmer plots of the two similarly structured probes are extremely different. The relative fluorescence intensity of ABA versus PA concentration shows the substitution of a linear slope with an upward

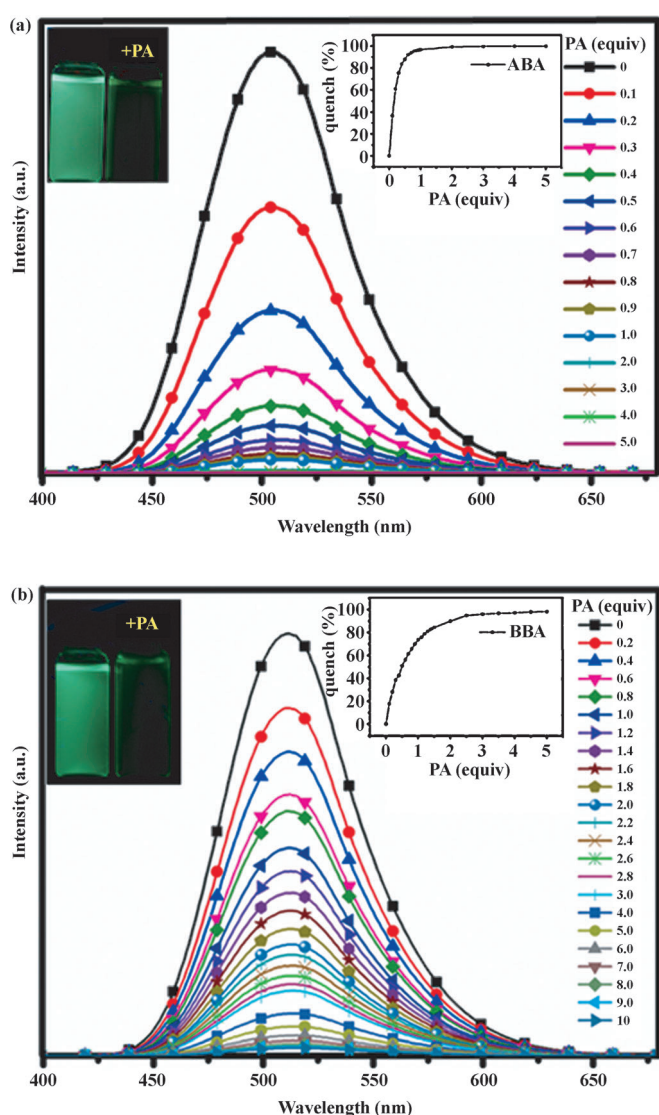


**Figure 2.** Change in the fluorescence of a) ABA in  $\text{H}_2\text{O}/\text{THF}$  (7:3 v/v) and b) BBA in  $\text{H}_2\text{O}/\text{THF}$  (6:4 v/v) upon the addition of PA ( $\lambda_{\text{ex}} = 375 \text{ nm}$ ). Inset, upper left: Visual fluorescence change of the probes before and after addition of PA. Inset, upper right: Fluorescence quenching percentage as a function of PA concentration. Concentration =  $1 \mu\text{M}$ .

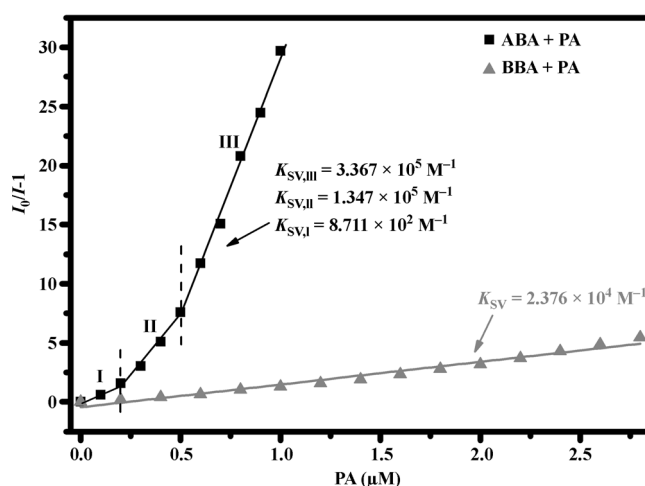


**Figure 3.** Plots of  $(I_0/I-1)$  values versus PA concentrations in a THF/water mixture (7:3 v/v for ABA, 6:4 v/v for BBA, respectively).  $I_0$  = peak intensity at  $[\text{PA}] = 0$ . Concentration =  $1 \mu\text{M}$ , excitation wavelength:  $375 \text{ nm}$ .

curve, thus indicating the super-amplification effect and superior binding ability.<sup>[3e]</sup> On the basis of the plots, the largest constants reach up to  $3.367 \times 10^5 \text{ M}^{-1}$ . However, that of BBA is linear with a quenching constant ( $K_{\text{SV}}$ ) of  $2.376 \times 10^4 \text{ M}^{-1}$ . At the same time, the calculated limit of detection (LoD,  $3\sigma/\text{slope}$ <sup>[3c]</sup>) for ABA and BBA were  $2.85 \times 10^{-7}$  and  $1.96 \times 10^{-6} \text{ M}$ , respectively. The results indicate that probe ABA is more sensitive than BBA. Because of the smaller steric hindrance, ABA was deemed to have a preferable performance for PA detection and higher Stern–Volmer constants.

The responses of the two probes in each mixed system with ten equivalents of a related nitro derivative were also studied. As shown in Figure 4, the emission intensity is almost unaffected in the presence of an excess amount of the selected nitro derivatives, thereby implying potential applications in real-world environmental conditions.

The interactions between the two probes and PA in solutions were further checked by means of  $^1\text{H}$  NMR spectroscopic

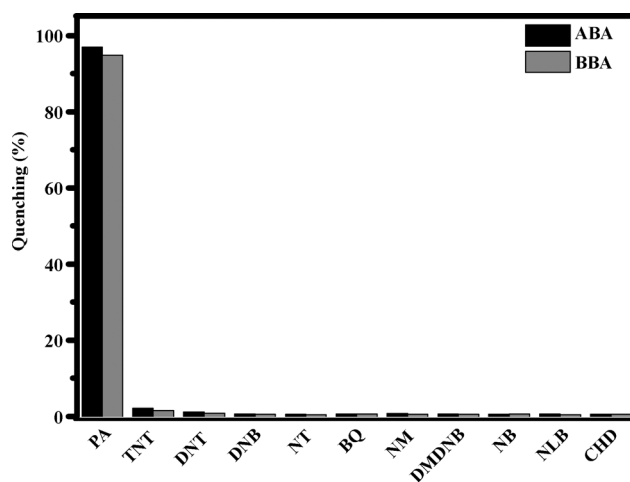


**Figure 4.** Extent of fluorescence quenching of ABA and BBA after addition of 10 equiv of various nitro derivatives in their  $\text{H}_2\text{O}/\text{THF}$  binary systems.

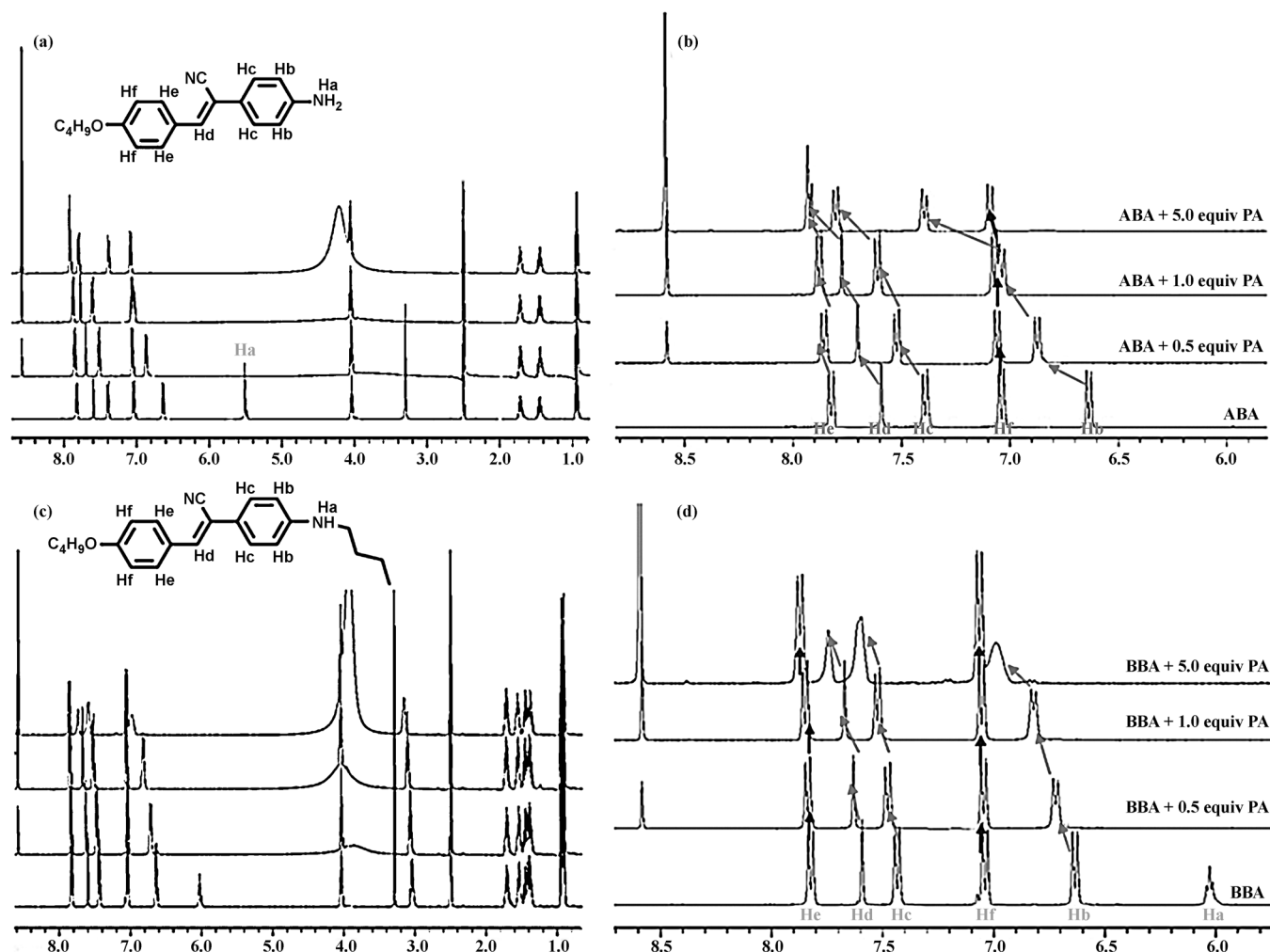


**Figure 5.** The whole and partial (for clarity)  $^1\text{H}$  NMR spectra (400 MHz) of probes a, b) ABA and c, d) BBA with PA (0, 0.5, 1.0, 5.0 equiv) in  $[\text{D}_6]\text{DMSO}$ .

titration experiments (Figure 5). The signals of the hydrogen atoms located on the aromatic rings were generally shifted downfield upon addition of PA (5 equiv). Among them, Hb, Hc, and Hd were clearly shifted, and the chemical shifts ( $\Delta\delta$ ) for ABA were 0.759, 0.414, and 0.342 ppm, and for BBA they were 0.367, 0.172, and 0.151 ppm, respectively. Meanwhile, the signals of the amino hydrogen atoms disappeared when PA was added to the probe solutions. These results imply that the protonation of an amino group by PA, the only reasonable site for protonation, resulted in the deshielding of the protons.<sup>[10a]</sup> The effects of pH on the two probes were also investigated to verify the quenching mechanism. The pH in 70 and 60% (v/v)  $\text{H}_2\text{O}/\text{THF}$  mixed solutions was 5.11 and 5.22 in the presence of five equivalents of PA, respectively. However, it was found that the fluorescence emission intensities of the two probes were almost unaffected throughout the pH range 3–12 (Figure S5 in the Supporting Information). These results indicated that the formation of host–guest complexes (ion pairs) between the probes and PA rather than the pH effects led to efficient fluorescence quenching when PA was introduced into the systems of the two probes.

To study the ionic interactions of the probes with PA, crystallographic studies of ABA and BBA with PA (ABAT and BBAT, respectively) were carried out (Figure 6). The formation of 1:1 host–guest complexes by the probe molecules and PA was confirmed by single-crystal X-ray analysis. The ABA and BBA cations were formed by the protonation of the amino groups, whereas the PA anion was formed by the deprotonation of the phenolic hydroxy group,<sup>[12]</sup> as revealed by the crystalline molecular structure. Analyzed results revealed that ABAT crystallized in orthorhombic system, space group  $Pbcn$  and BBAT crystallized in a triclinic system, space group  $P\bar{1}$ . More crystallographic data about the two single crystals is summarized in Tables S1 and S2 of the Supporting Information. From Figure 7a,b, we can observe that five ABA cations are connected to one picrate through ten hydrogen-bond interactions and each ABA cation links two picrates and three other ABA cations through 12 hydrogen-bond interactions. The linkages between the picrate and ABA cation are  $\text{C}-\text{H}\cdots\text{O}$  or  $\text{N}-\text{H}\cdots\text{O}$  interactions, whereas the linkages between the cations are  $\text{N}-\text{H}\cdots\text{N}$  interactions. The D–A distances and D–H $\cdots$ A angles of these weak interactions vary from 1.835 to 2.713 Å and from 89.575 to



plexes are dominated by the orbitals from the cyanostilbene parts and the PA anion parts, respectively, thus leading to a completely inhibited ICT in the  $\pi$ -conjugated moieties. These results indicate that the inhibited ICT caused by the effective protonation of amino groups and deprotonation of PA is important for the fluorescence quenching.<sup>[3c, 4c]</sup> The time-resolved emission spectra studies of ABA and BBA with different amounts of PA were also studied to gain further insight into the quenching mechanism. Before the addition of PA, the average fluorescence lifetimes of ABA and BBA were 0.97 and 1.13 ns, respectively. After the addition of 1, 5, and 10 equivalents of PA, the average lifetimes (0.85, 0.77, and 0.49 ns for ABA; 1.06, 0.96, and 0.87 ns for BBA) were lowered, thus suggesting the dynamic quenching process occurred through electron transfer from the electron-rich fluorophore to the exceedingly electron-deficient PA.<sup>[4a]</sup> Cyclic voltammetry studies of ABA and BBA also support the electron-transfer mechanism (Figure S11 in the Supporting Information). The higher LUMO of ABA (-3.40 eV) and BBA (-3.35 eV) allows the electron to transfer effectively to the lower energy of PA (-3.89 eV).<sup>[3b, 13]</sup> The sensing mechanism of probes ABA and BBA toward PA are illustrated in Scheme 1.

To apply the detection in a direct and available method, test strips were prepared with a method of dip-coating of the probes on a Whatmann filter, then dried under vacuum. As shown in Figure S12 of the Supporting Information, the test strips offer soft and visual detection of PA based on the fluorescence quenching upon dipping the test strips into PA solution under the UV lamp illumination. At the same time, the change from strong emission to nonluminescence when a small quantity of PA was absorbed on the probe-impregnated TLC plates provides another easier and more convenient detection method. In addition, the different strength of the dark spots provided an immediate visualization of the traces of PA.

## Conclusion

In conclusion, by combining amine and secondary amine groups with  $\alpha$ -cyanostilbene, we have successfully developed two novel small molecular chemosensors for selective and sensitive detection of PA in mixed aqueous media. The easy protonation of the amine group and ensuing formation of ionic pairs between PA and molecular sensors enhanced the fluorescence quenching effect. These kinds of molecules could be applied under natural environmental conditions for efficient detection of PA in both solvent and solid states. The present strategy is instructive, and we anticipate that it could be extended to the design of other effective chemosensors.

## Experimental Section

### Materials and instruments

The commercially available chemicals were used without further purification. All of the solvents used were purified by conventional methods before use. <sup>1</sup>H and <sup>13</sup>C NMR spectra were recorded using

a Bruker 400 MHz NMR spectrometer with CDCl<sub>3</sub> or [D<sub>6</sub>]DMSO as solvent and calibrated using tetramethylsilane (TMS) as an internal reference. The following data are reported: chemical shifts ( $\delta$ ) [ppm], multiplicity, coupling constants *J* [Hz], integration, and interpretation. UV/Vis absorption spectra were recorded using a TU-1901 spectrometer from Beijing Purkinje General Instrument Co., Ltd with samples in solution and a quartz cuvette (path length 1 cm). Fluorescence measurements were carried out using an Edinburgh FLS920 fluorescence spectrometer equipped with a 450 W Xe lamp and a time-correlated single-photon counting (TCSPC) card. All the fluorescence spectra were collected. The fluorescence decay experiments were measured using a Horiba FluoroMax-4 instrument, and DAS6 v6.6 analysis software was used to fit the data. FTIR spectra were obtained in KBr discs using a Nicolet 380 FTIR spectrometer in the 4000–400 cm<sup>-1</sup> region. Powder X-ray diffraction patterns were obtained using an MXP 18AHF X-ray diffractometer in the 5–90°  $2\theta$  range with graphite-monochromated Cu<sub>K $\alpha$</sub>  radiation. Fluorescence images were obtained using a digital camera (Nikon D7000). Silica gel 60 (60–120 mesh) was used for column chromatography.

**Caution!** PA, TNT, DNT, and other nitroaromatics should be used with extreme care using the best safety precautions owing to their highly explosive character. They should be handled only in small quantities.

### Theoretical calculations

To further investigate the solvent effects and gain an additional understanding of the fluorescence behaviors of ABA and BBA with PA, we carried out quantum chemical calculations on the basis of density functional theory. The geometries of ABA, BBA, ABAT, and BBAT were obtained using the Gaussian 09 package by adopting the B3LYP (Becke's three-parameter hybrid exchange-correlation (x-c) functional) method with the 6-31G\* basis set to determine the lowest-energy structures. Time-dependent (TD)-DFT calculations were carried for the necessary excitation energies at the optimized geometries.<sup>[14, 15]</sup>

### Single-crystal X-ray diffraction

Data for single crystals were collected using a Siemens Smart 1000 CCD diffractometer. The determination of unit-cell parameters and data collections were performed using Mo<sub>K $\alpha$</sub>  radiation ( $\lambda = 0.71073$  Å) in  $\omega$  scan mode at 293(2) K. Unit-cell dimensions were obtained with least-squares refinements, and all structures were solved by direct methods using SHELXS-97. The other non-hydrogen atoms were located in successive difference Fourier syntheses. The final refinement was performed by using full-matrix least-squares methods with anisotropic thermal parameters for non-hydrogen atoms on *F*<sup>2</sup>. The hydrogen atoms were added theoretically.

### Synthesis of compound 1

For compound 1, the synthetic route was modified according to the reported procedure.<sup>[16]</sup>

### Synthesis of compound 2

Compound 2 was synthesized according to our reported literature procedure.<sup>[17]</sup> <sup>1</sup>H NMR (CDCl<sub>3</sub>, 400 MHz):  $\delta = 10.02$  (s, 1 H; OH), 7.75 (d, *J* = 8.8 Hz, 2 H; ArH), 7.54 (s, 1 H; CH), 7.36 (d, *J* = 8.4 Hz, 2 H; ArH), 6.66 (d, *J* = 8.8 Hz, 2 H; ArH), 6.62 (d, *J* = 8.8 Hz, 2 H; ArH), 5.42 ppm (s, 2 H; NH<sub>2</sub>); <sup>13</sup>C NMR (CDCl<sub>3</sub>, 400 MHz):  $\delta = 158.9, 149.5,$

137.1, 130.5, 137.1, 129.7, 128.3, 125.4, 121.3, 118.9, 115.7, 115.6, 105.8 ppm; FTIR (KBr):  $\tilde{\nu}$  = 3434 (vs), 3341 (vs), 3285 (vs), 2215 (m), 1793 (w), 1624 (m), 1605 (vs), 1521 (vs), 1447 (m), 1400 (m), 1281 (m), 1258 (s), 1179 (s), 890 (w), 825 cm<sup>-1</sup> (m).

### Synthesis of probes ABA and BBA

For the synthesis of compounds (Z)-2-(4-aminophenyl)-3-(4-butoxyphenyl)acrylonitrile (ABA) and (Z)-3-(4-butoxyphenyl)-2-[4-(butylamino)phenyl]acrylonitrile (BBA), a mixture of compound **2** (1.0 g, 4.23 mmol) dissolved in DMF (10 mL) and NaOH (339 mg, 8.46 mmol) was stirred for 15 min at RT. Then 1-bromobutane (928.8 mg, 8.47 mmol) was added, and the mixture was sequentially stirred for 12 h at 90 °C. The mixture was poured into water (500 mL) and extracted with ethyl acetate (100 mL) three times. Finally, after silica gel column chromatography (*n*-hexane/EtOAc 6:1), the two crude products were recrystallized from ethanol and water to give the yellow powder ABA (824.3 mg, 66.3%) and BBA (292.7 mg, 19.9%).

**Compound ABA:** <sup>1</sup>H NMR ([D<sub>6</sub>]DMSO, 400 MHz):  $\delta$  = 7.83 (d, *J* = 8.8 Hz, 2H; ArH), 7.60 (s, 1H; CH), 7.39 (d, *J* = 8.4 Hz, 2H; ArH), 7.04 (d, *J* = 8.8 Hz, 2H; ArH), 6.64 (d, *J* = 8.4 Hz, 2H; ArH), 5.54 (s, 2H; NH<sub>2</sub>), 4.03 (t, *J* = 6.4 Hz, 2H; CH<sub>2</sub>), 1.71 (t, *J* = 6.8 Hz, 2H; CH<sub>2</sub>), 1.44 (q, 2H; CH<sub>2</sub>), 0.94 ppm (t, 3H; CH<sub>3</sub>); <sup>13</sup>C NMR ([D<sub>6</sub>]DMSO, 400 MHz):  $\delta$  = 159.7, 149.7, 136.6, 130.3, 126.8, 126.4, 121.1, 118.7, 114.7, 113.9, 107.8, 67.3, 30.6, 18.7, 13.6 ppm; FTIR (KBr):  $\tilde{\nu}$  = 3455 (vs), 3360 (vs), 3031 (s), 2956 (m), 2920 (s), 2852 (m), 2213 (m), 1797 (w), 1639 (s), 1606 (vs), 1564 (m), 1515 (s), 1466 (s), 1388 (w), 1357 (w), 1298 (s), 1257 (s), 1174 (s), 1123 (s), 1069 (m), 1034 (m), 1002 (m), 896 (w), 827 (m), 803 (w), 766 (w), 721 (w), 628 cm<sup>-1</sup> (w).

**Compound BBA:** <sup>1</sup>H NMR (CDCl<sub>3</sub>, 400 MHz):  $\delta$  = 7.83 (d, *J* = 8.4 Hz, 2H; ArH), 7.60 (s, 1H; CH), 7.45 (d, *J* = 8.4 Hz, 2H; ArH), 7.03 (d, *J* = 8.4 Hz, 2H; ArH), 6.64 (d, *J* = 8.0 Hz, 2H; ArH), 6.06 (s, 1H; NH), 4.02 (t, 2H; CH<sub>2</sub>), 3.03 (t, 2H; CH<sub>2</sub>), 1.69 (m, 2H; CH<sub>2</sub>), 1.52 (m, 2H; CH<sub>2</sub>), 1.40 (m, 4H; 2CH<sub>2</sub>), 0.92 ppm (t, 6H; 2CH<sub>3</sub>); <sup>13</sup>C NMR (CDCl<sub>3</sub>, 400 MHz):  $\delta$  = 160.5, 147.1, 138.5, 130.7, 127.0, 126.8, 125.0, 118.9, 115.1, 114.8, 108.6, 68.2, 53.5, 31.6, 29.1, 25.7, 22.6, 14.1, 13.9 ppm; FTIR (KBr):  $\tilde{\nu}$  = 3377 (vs), 3027 (s), 2958 (vs), 2930 (vs), 2871 (vs), 2211 (s), 1609 (vs), 1524 (vs), 1475 (s), 1418 (w), 1335 (vs), 1269 (vs), 1254 (vs), 1179 (vs), 1146 (w), 1124 (w), 1067 (w), 1309 (m), 1008 (m), 970 (w), 938 (m), 891 (vs), 767(w), 740 (w), 635 cm<sup>-1</sup> (w).

CCDC-931697 (**2**), -975117 (ABA), -937566 (BBA), -987145 (ABAT), and -987082 (BBAT) contain the supplementary crystallographic data for this paper. These data can be obtained free of charge from The Cambridge Crystallographic Data Centre via [www.ccdc.cam.ac.uk/data\\_request/cif](http://www.ccdc.cam.ac.uk/data_request/cif).

### Acknowledgements

This work was supported by the National Natural Science Foundation of China (21101001, 50873001, and 61107014), the Natural Science Foundation of Anhui Province (1208085MB21), the 211 Project of Anhui University, the Team for Scientific Innovation Foundation of Anhui Province (2006KJ007TD), and a strategic faculty grant in material science from the Swedish government (SFO-Mat-Liu # 2009-00971).

**Keywords:** amines • fluorescence • host-guest systems • ion pairs • sensors

- [1] a) A. J. Lan, K. H. Li, H. H. Wu, D. H. Olson, T. J. Emge, W. Ki, M. C. Hong, J. Li, *Angew. Chem.* **2009**, *121*, 2370–2374; *Angew. Chem. Int. Ed.* **2009**, *48*, 2334–2338; b) K. K. Kartha, S. S. Babu, S. Srinivasan, A. Ajayaghosh, *J. Am. Chem. Soc.* **2012**, *134*, 4834–4841; c) G. He, N. Yan, J. Y. Yang, H. Wang, L. P. Ding, S. Yin, Y. Fang, *Macromolecules* **2011**, *44*, 4759–4766; d) K. Zhang, H. B. Zhou, Q. S. Mei, S. H. Wang, G. J. Guan, R. Y. Liu, J. Zhang, Z. P. Zhang, *J. Am. Chem. Soc.* **2011**, *133*, 8424–8427; e) J. L. Pablos, M. Trigo-López, F. Serna, F. C. García, J. M. García, *Chem. Commun.* **2014**, *50*, 2484–2487; f) S. Madhu, A. Bandela, M. Ravikanth, *RSC Adv.* **2014**, *4*, 7120–7123.
- [2] a) J. Akhavan, The chemistry of explosives, *Royal Society of Chemistry* **2011**; b) H. Muthurajan, R. Sivabalan, M. B. Talawar, S. N. Asthana, *J. Hazard. Mater.* **2004**, *112*, 17–33; c) D. T. Meredith, O. C. Lee, *J. Am. Pharm. Assoc.* **1939**, *28*, 369; d) B. Roy, A. K. Bar, B. Gole, P. S. Mukherjee, *J. Org. Chem.* **2013**, *78*, 1306–1310; e) V. Bhalla, S. Kaur, V. Vij, M. Kumar, *Inorg. Chem.* **2013**, *52*, 4860–4865.
- [3] a) P. C. Ashbrook, T. A. Houts, *Chem. Health Safety* **2003**, *10*, 27; b) N. Venkatramaiah, S. Kumar, S. Patil, *Chem. Commun.* **2012**, *48*, 5007–5009; c) Y. Q. Xu, B. H. Li, W. W. Li, J. Zhao, S. G. Sun, Y. Pang, *Chem. Commun.* **2013**, *49*, 4764–4766; d) V. Pimienta, R. Etchenique, T. Buhse, *J. Phys. Chem. A* **2001**, *105*, 10037–10044; e) J. Li, J. Liu, J. W. Y. Lam, B. Z. Tang, *RSC Adv.* **2013**, *3*, 8193–8196.
- [4] a) N. Dey, S. K. Samanta, S. Bhattacharya, *ACS Appl. Mater. Interfaces* **2013**, *5*, 8394–8400; b) V. Bhalla, A. Gupta, M. Kumar, *Org. Lett.* **2012**, *14*, 3112–3115; c) M. Kumar, S. I. Reja, V. Bhalla, *Org. Lett.* **2012**, *14*, 6084–6087.
- [5] G. He, H. N. Peng, T. H. Liu, M. N. Yang, Y. Zhang, Y. Fang, *J. Mater. Chem.* **2009**, *19*, 7347–7353.
- [6] V. Bhalla, A. Gupta, M. Kumar, D. S. Rao, S. K. Prasad, *ACS Appl. Mater. Interfaces* **2013**, *5*, 672–679.
- [7] a) S. J. Toal, W. C. Trogler, *J. Mater. Chem.* **2006**, *16*, 2871–2883; b) B. W. Xu, X. F. Wu, H. B. Li, H. Tong, L. X. Wang, *Macromolecules* **2011**, *44*, 5089–5092.
- [8] Y. Y. Long, H. B. Chen, H. M. Wang, Z. Peng, Y. F. Yang, G. Q. Zhang, N. Li, F. Liu, J. Pei, *Anal. Chim. Acta* **2012**, *744*, 82–91.
- [9] a) Z. F. An, C. Zheng, R. F. Chen, J. Yin, J. J. Xiao, H. F. Shi, Y. Tao, Y. Qian, W. Huang, *Chem. Eur. J.* **2012**, *18*, 15655–15661; b) D. D. Li, J. Z. Liu, R. T. K. Kwok, Z. Q. Liang, B. Z. Tang, J. H. Yu, *Chem. Commun.* **2012**, *48*, 7167–7169.
- [10] a) V. Vij, V. Bhalla, M. Kumar, *ACS Appl. Mater. Interfaces* **2013**, *5*, 5373–5380; b) T. H. Liu, L. L. Ding, G. He, Y. Yang, W. L. Wang, Y. Fang, *ACS Appl. Mater. Interfaces* **2011**, *3*, 1245–1253.
- [11] a) B.-K. An, S.-K. Kwon, S.-D. Jung, S. Y. Park, *J. Am. Chem. Soc.* **2002**, *124*, 14410–14415; b) J. W. Chung, Y. You, H. S. Huh, B.-K. An, S.-J. Yoon, S. H. Kim, S. Y. Lee, S. Y. Park, *J. Am. Chem. Soc.* **2009**, *131*, 8163–8172; c) C.-W. Chang, C. J. Bhongale, C.-S. Lee, W.-K. Huang, C.-S. Hsu, E. W.-G. Diao, *J. Phys. Chem. C* **2012**, *116*, 15146–15154; d) B. R. Gao, H. Y. Wang, Y. W. Hao, L. M. Fu, H. H. Fang, Y. Jiang, L. Wang, Q. D. Chen, H. Xia, L. Y. Pan, Y. G. Ma, H. B. Sun, *J. Phys. Chem. B* **2010**, *114*, 128–134.
- [12] a) Y. Peng, A. J. Zhang, M. Dong, Y. W. Wang, *Chem. Commun.* **2011**, *47*, 4505–4507; b) Y. Zhang, Y. Guo, Y. H. Joo, D. A. Parrish, J. M. Shreeve, *Chem. Eur. J.* **2010**, *16*, 10778–10784.
- [13] H. Sohn, M. J. Sailor, D. Magde, W. C. Trogler, *J. Am. Chem. Soc.* **2003**, *125*, 3821.
- [14] Gaussian 09, Revision B.01, M. J. Frisch, G. W. Trucks, H. B. Schlegel, G. E. Scuseria, M. A. Robb, J. R. Cheeseman, G. Scalmani, V. Barone, B. Menonucci, G. A. Petersson, H. Nakatsuji, M. Caricato, X. Li, H. P. Hratchian, A. F. Izmaylov, J. Bloino, G. Zheng, J. L. Sonnenberg, M. Hada, M. Ehara, K. Toyota, R. Fukuda, J. Hasegawa, M. Ishida, T. Nakajima, Y. Honda, O. Kitao, H. Nakai, T. Vreven, J. A. Montgomery, Jr., J. E. Peralta, F. Ogliaro, M. Bearpark, J. J. Heyd, E. Brothers, K. N. Kudin, V. N. Staroverov, R. Kobayashi, J. Normand, K. Raghavachari, A. Rendell, J. C. Burant, S. S. Iyengar, J. Tomasi, M. Cossi, N. Rega, J. M. Millam, M. Klene, J. E. Knox, J. B. Cross, V. Bakken, C. Adamo, J. Jaramillo, R. Gomperts, R. E. Stratmann, O. Yazyev, A. J. Austin, R. Cammi, C. Pomelli, J. W. Ochterski, R. L. Martin, K. Morokuma, V. G. Zakrzewski, G. A. Voth, P. Salvador, J. J. Dannenberg,

- S. Dapprich, A. D. Daniels, Ö. Farkas, J. B. Foresman, J. V. Ortiz, J. Cio-slawski, D. J. Fox, Gaussian, Inc., Wallingford CT, **2009**.
- [15] a) A. D. Becke, *J. Chem. Phys.* **1993**, *98*, 5648–5652; b) B. Miehlich, A. Savin, H. Stoll, H. Preuss, *Phys. Rev. Lett.* **1989**, *157*, 200–206; c) R. Bauernschmitt, R. Ahlrichs, *Chem. Phys. Lett.* **1996**, *256*, 454–464; d) M. E. Casida, C. Jamorski, K. C. Casida, D. R. Salahub, *J. Chem. Phys.* **1998**, *108*, 4439–4449.
- [16] B. Kim, H. R. Yeom, W. Y. Choi, J. Y. Kim, C. Yang, *Tetrahedron* **2012**, *68*, 6696–6700.
- [17] H. B. Lu, L. Z. Qiu, G. Y. Zhang, A. X. Ding, W. B. Xu, G. B. Zhang, X. H. Wang, L. Kong, Y. P. Tian, J. X. Yang, *J. Mater. Chem. C* **2014**, *2*, 1386–1389.

---

Received: March 26, 2014  
Published online on July 31, 2014